AD-A173 814 DISTRIBUTION ANALYSIS OF MAJOR AND TRACE ELEMENTS THROUGH SEMICONDUCTOR L (U) AEROSPACE CORP EL SEGUNDO CA MATERIALS SCIENCES LAB A A GALUSKA ET AL 15 AUG 86 1/1

UNCLASSIFIED TR-0086(6935-05)-1 SD-TR-86-53 F/G 20/12 NL

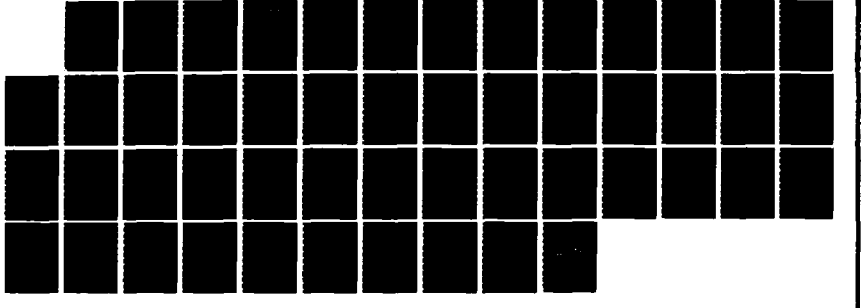

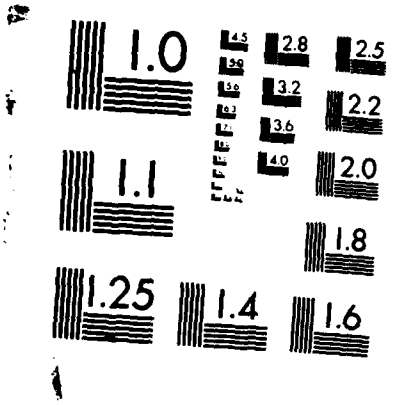

REPORT SD-TR-86-53

Distribution Analysis of Major and Trace Elements Through Semiconductor Layers of Changing Matrix Using SIMS

A. A. GALUSKA
Materials Sciences Laboratory
Laboratory Operations
The Aerospace Corporation
El Segundo, CA 90245

and

G. H. MORRISON
Department of Chemistry
Cornell University
Ithaca, NY 14853

15 August 1986

Prepared for

SPACE DIVISION
AIR FORCE SYSTEMS COMMAND
Los Angeles Air Force Station
P.O. Box 92960, Worldway Postal Center
Los Angeles, CA 90009-2960

This report was submitted by The Aerospace Corporation, El Segundo, CA 90245, under Contract No. F04701-85-C-0086 with the Space Division, P.O. Box 92960, Worldway Postal Center, Los Angeles, CA 90009-2960. It was reviewed and approved for The Aerospace Corporation by R. W . Fillers, Director, Materials Sciences Laboratory. Lt Ethel Dotts, SD/YUE, was the project officer for the Mission-Oriented Investigation and Experimentation (MOIE) Program.

This report has been reviewed by the Public Affairs Office (PAS) and is releasable to the National Technical Information Service (NTIS). At NTIS, it will be available to the general public, including foreign nationals.

This technical report has been reviewed and is approved for publication. Publication of this report does not constitute Air Force approval of the report's findings or conclusions. It is published only for the exchange and stimulation of ideas.

Ethel Dotts 21 Jul 86

ETHEL DOTTS, Lt, USAF
MOIE Project Officer
SD/YUE

Joseph Hess

JOSEPH HESS, GM-15
Director, AFSTC West Coast Office
AFSTC/WCO OL-AB

UNCLASSIFIED

SECURITY CLASSIFICATION OF THIS PAGE (When Data Entered)

REPORT DOCUMENTATION PAGE	READ INSTRUCTIONS BEFORE COMPLETING FORM
1. REPORT NUMBER: SD-TR-86-53	2. GOVT ACCESSION NO.: AD-A173 814
	3. RECIPIENT'S CATALOG NUMBER:
4. TITLE (and Subtitle): DISTRIBUTION ANALYSIS OF MAJOR AND TRACE ELEMENTS THROUGH SEMICONDUCTOR LAYERS OF CHANGING MATRIX USING SIMS	5. TYPE OF REPORT & PERIOD COVERED:
	6. PERFORMING ORG. REPORT NUMBER: TR-0086(6935-05)-1
7. AUTHOR(s): Alan A. Galuska and G. H. Morrison	8. CONTRACT OR GRANT NUMBER(s): F04701-85-C-0086
9. PERFORMING ORGANIZATION NAME AND ADDRESS: The Aerospace Corporation, El Segundo, CA 90245	10. PROGRAM ELEMENT, PROJECT, TASK AREA & WORK UNIT NUMBERS:
11. CONTROLLING OFFICE NAME AND ADDRESS: Space Division, Los Angeles Air Force Station, Los Angeles, CA 90009-2960	12. REPORT DATE: 15 August 1986
	13. NUMBER OF PAGES: 46
14. MONITORING AGENCY NAME & ADDRESS (if different from Controlling Office):	15. SECURITY CLASS. (of this report): Unclassified
	15a. DECLASSIFICATION/DOWNGRADING SCHEDULE:

16. DISTRIBUTION STATEMENT (of this Report)

Approved for public release; distribution unlimited

17. DISTRIBUTION STATEMENT (of the abstract entered in Block 20, if different from Report)

18. SUPPLEMENTARY NOTES

19. KEY WORDS (Continue on reverse side if necessary and identify by block number)

Secondary Ion Mass Spectrometry
Thin Film and Interface Characterization

20. ABSTRACT (Continue on reverse side if necessary and identify by block number)

Secondary ion mass spectrometry (SIMS) is often used to monitor elemental distributions in solids and at solid interfaces. The technique is highly sensitive for most elements and has good depth resolution. However, the complexity of the sputtering event has made quantitative analysis difficult, especially in multimatrix samples where changing matrix effects are encountered. Because of the increasing importance of multilayer-multimatrix

DD FORM 1473 (FACSIMILE)

UNCLASSIFIED

SECURITY CLASSIFICATION OF THIS PAGE (When Data Entered)

19. KEY WORDS (Continued)

20. ABSTRACT (Continued)

samples in semiconductor device technology, matrix effect calibration for quantitative SIMS analyses in these samples is essential. In this report, the current status of quantitative SIMS analysis in layered multimatrix samples is presented. The basics of SIMS quantification and theories describing matrix effects will be reviewed, matrix effect calibration and depth profile corrections for $Al_xGa_{1-x}As$ multilayers will be examined, a method of extending these calibrations to the remaining IIIA-VA semiconductors will be presented, and future trends in matrix effect calibration and depth profile correction will be discussed.

CONTENTS

A-1

FIGURES

TABLES

I. INTRODUCTION

In the past, semiconductor technology was largely limited to silicon technology. Electronic devices were rather large and simple in construction. Current trends in semiconductor technology involve the fabrication of smaller (≤ 1.0 μm) and more complex electronic structures composed of an increasing variety of materials. In particular, microwave and optoelectronic devices composed of group IIIA-VA and IIB-VIIA compound semiconductors are rapidly being developed using growth techniques such as molecular beam epitaxy (MBE) and metal-organic chemical vapor deposition (MOCVD). An increasing number of these compound semiconductor devices are making use of superlattice structures, alternating thin lattice-matched semiconductor layers of varying composition (Fig. 1).

There is a tremendous need for major and trace element quantification through these semiconductor structures. There are a few surface analysis techniques, such as Rutherford backscattering spectrometry (RBS) and Auger electron spectrometry (AES), which have the necessary depth resolution ($\leq$ 100 Å) and sensitivity to examine the distribution of the major elements. However, secondary ion mass spectrometry (SIMS) is the only technique capable of simultaneously measuring major and also trace (~ 1 ppm) elemental depth distributions. Consequently, SIMS has great potential for characterization of these semiconductor structures.

Because of the complexity of the sputtering and ion emission processes, quantitative SIMS analyses are difficult to obtain. Thus the full potential of SIMS has not been realized. Every measurement is influenced by the uncertainty resulting from statistical fluctuations in the measured secondary ion current and systematic uncertainties related to experimental conditions as well as sample characteristics. For trace elements in homogeneous matrices, these sources of error can generally be eliminated or reduced so that quantitative measurements (~ 15%) can be made. Conversely, quantitative analysis in heterogeneous matrices has been severely limited because of the uncharacterized variation of secondary ion yields and sputtering yields with

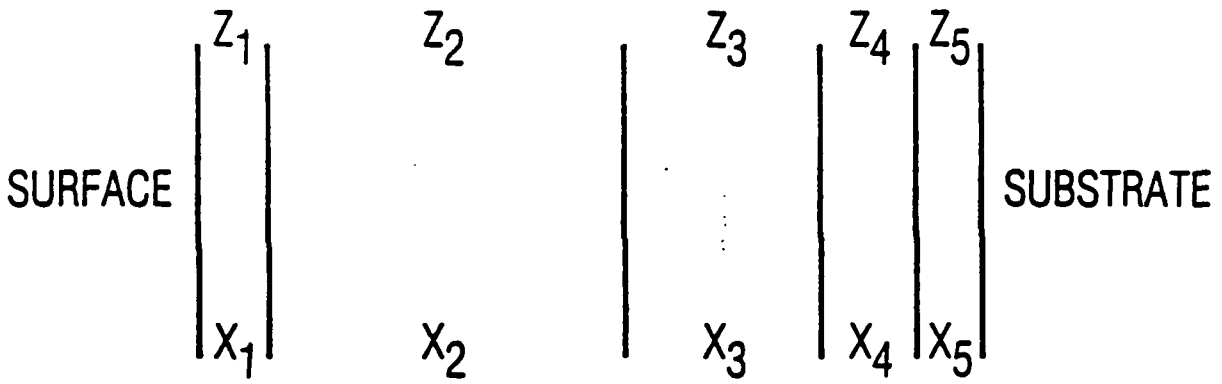

Fig 1. A Hypothetical $Al_xGa_{1-x}As$ Superlattice. The thickness Z of the layers can vary from several angstroms to several microns while x can be varied from 0 to 1.[38]

sample matrix (matrix effects). A depth profile of a sample composed of more than one matrix (in particular, layers of different matrices stacked on top of each other) becomes distorted by the variation of secondary ion yields and sputtering yields with matrix. Signal and time are no longer proportional to concentration and depth, respectively.

Despite these difficulties, the proper calibration of ion yields and sputtering yields with matrix can make quantitative SIMS depth profiling possible for these multilayer-multimatrix samples. In this report, procedures for quantifying SIMS depth profiles through layers of IIIA-VA semiconductors will be described. The basics of SIMS quantification and theories describing matrix effects will be reviewed, matrix effect calibrations and depth profile corrections for $Al_xGa_{1-x}As$ multilayers will be examined, a method of extending these calibrations to the remaining IIIA-VA semiconductors will be presented, and future trends in matrix effect calibration and depth profile correction will be discussed.

II. SIMS QUANTIFICATION

When a solid surface is bombarded by energetic (5-20 keV) primary ions, the elements present are sputtered primarily as neutrals, although positive ions, negative ions, and polyatomic ions are also formed. Typically, only the secondary ion intensities of the monomeric ions, either M^+ or M^-, are used in SIMS elemental quantification. The relationship between the number of analyte ions detected, I_M (counts), and the isotopically corrected analyte concentration, C_M (atoms/cm^3), in the sample surface can be defined as

$$I_M = \tau_M C_M S_M J A_o T N^{-1} \quad (1)$$

where τ_M is the useful ion yield, S_M is the sputtering yield, J is the current density (ions/cm^2-sec), and A is the analysis area (cm^2). T is the analysis time (sec), and N is the atomic density (atoms/cm^3) of the sample matrix. The useful ion yield is defined as the ratio of the number of analyte ions, $M^\pm$, detected to the number of analyte atoms sputtered from the specimen. Useful ion yields are also defined as the product of the probability of $M^\pm$ formation ($\beta^\pm$) and the transmission efficiency (η). The sputtering yield is defined as the average number of atoms sputtered by each incident primary ion. It is assumed that the elemental components of the sputtering yield are proportional to the bulk elemental concentrations.

The difficulty in solving Eq. (1) for analyte concentration is that useful ion yields and sputtering yields are influenced by a variety of factors, and can vary drastically from sample to sample. Useful ion yields can vary by orders of magnitude for different elements in the same matrix and for the same element in different matrices.[1-4] In addition, useful positive ion yields are increased by the presence of electronegative elements such as oxygen,[5] and useful negative ion yields are increased by the presence of electropositive elements such as cesium.[6] Sputtering yields are also different for different elements in the same or different sample matrices. Sputtering yields are influenced by the following: primary ion mass, energy

and density, mass of the target atoms, sample crystallinity and orientation, surface-binding energy, and the angle of incidence between the primary ion beam and the sample surface.[7-9] Consequently, useful ion yields and sputtering yields must be determined for every element and sample matrix. In addition, because of the fluctuation of experimental conditions with time, these values must be determined each time quantification is performed in the same sample matrix.

For pure elemental matrices, sputtering yields can be determined experimentally from the sputtering rate $\dot{z}$ (cm/sec). After sputtering, the depth of the sputtered crater is measured using a profilometer or an optical interferometer. If this depth is divided by the sputtering time interval, the average sputtering rate can be obtained. If the approximation is made that the crater walls behave as step functions, the sputtering yield may be determined from

$$S = \dot{z} A N/i_p \tag{2}$$

where A is the crater area (cm^2), and i_p is the primary beam current (ions/sec).

In matrices of more than one element, differences in elemental sputtering yields (preferential sputtering) result in composition changes in the near surface region.[10,11] Elements which sputter slowly are enriched at the surface while elements which sputter rapidly are depleted from the surface. These compositional changes usually occur over a short depth increment (approximately twice the range of the primary ion) after which a steady state condition is reached. At this point, the elemental components of the sputtering yield are proportional to the bulk elemental concentrations. Once this steady state condition has been reached, Eq. (2) can be incorporated into Eq. (1) to obtain a more practical form of the ion intensity equation.

$$I_M = \tau_M C_M \dot{z} A_o T \tag{3}$$

Equations 1 and 3 can now be solved for the analyte concentration providing τ_M can be accurately determined. Useful ion yields can be approximated using semitheoretical techniques,[12-16] but they are most accurately determined using homogeneous bulk standards or ion implanted standards[17-20] fabricated from the same matrix as the unknown sample.

Although practical ion yields can be determined from standards, they can change quite dramatically between analyses. Secondary ion collection and instrumental transmission are influenced by operator adjustment and indeterminate instrumental fluctuations that occur during routine operation. To reduce this effect, it is common practice to use relative sensitivity factors (RSF), as given by Eq. (4), in which the τ of an analyte is ratioed to that of a reference element of known concentration in the sample matrix.

$$\begin{aligned} RSF &= \tau_a/\tau_{ref} \\ &= (I_a\ C_{ref})/(I_{ref}\ C_a) \end{aligned} \tag{4}$$

The normalization procedure is designed to minimize the influence of instrumental variations.

III. MATRIX EFFECTS

The fabrication of external and internal standards by ion implantation has provided an accurate (15% relative standard deviation) means of quantifying trace element distributions in homogeneous matrices. However, because of the uncharacterized variation of secondary ion yields and sputtering yields with matrix composition (matrix effects), the quantitative SIMS analysis of heterogeneous matrices remains a problem. To overcome this difficulty, the mechanisms underlying matrix effects must be more clearly understood. Several factors are known to influence matrix effects. These include the bulk matrix composition and the surface concentration of reactive species (electronegative elements such as oxygen or electropositive elements such as cesium), which can either be adsorbed from the sample chamber during analysis or implanted as a primary ion. Several explanations for matrix effects, which depend to varying extents on the bulk composition and the reactive species concentrations have been proposed. The sputtering yield, compositional, and oxide bond approaches to matrix effect calibration will be presented and briefly discussed.

A. SPUTTERING YIELD APPROACH

The sputtering yield approach to matrix effect calibration is based on the fact that positive and negative ion yields are greatly enhanced by the incorporation of oxygen or cesium, respectively, in the sputtered surface. Deline et al.[21-23] state that for reactive beam sputtering, "ion yield matrix effects arise solely from variations in the substrate sputtering yields." They justify this statement by asserting that implanted oxygen and cesium are responsible for the observed matrix effects, and that the equilibrium concentration, [R], of these reactive species is determined by the sputtering yield, S.

The relationship between [R] and S is derived from equations describing ion implantation during sputtering:[24,25]

$$[R] = \alpha\ N/S \qquad (5)$$

$$C_s \tilde{=} [R]/([R] + N) = \alpha/(\alpha + S) \quad (6)$$

where α is the accommodation coefficient (which equals 1 - B, where B is the backscattering coefficient); N is the atomic density of the sample surface; and C_S is the atomic fraction of implanted projectiles in the surface. In their declaration, Deline et al. assume that $\alpha = 1$, that N and S are constant, and that there is no preferential sputtering. In their experiments, they make the further assumption that when primary current density is constant, the sputtering rate is approximately proportional to the sputtering yield regardless of N.

The result of these approximations is the relationship

$$\tau \propto [R] \propto (1/S)^y \propto (1/\overset{o}{z})^y_J = \text{const} \quad (7)$$

where y is a constant determined experimentally for each analyte. Plots of log (τ) versus log ($1/\overset{o}{z}$) obtained by Deline et al.[21-23] and others[26] for various elements have been roughly linear. However, the sputtering yield approach has been severely criticized[27-30] because of the many unjustified assumptions that are made. Various attempts to experimentally determine the relationship between [R] and S using Auger spectroscopy have both supported and contradicted the proposed relationship.[23,28-30] It is unclear when the sputtering yield approach applies or does not apply.

B. COMPOSITIONAL APPROACH

The compositional approach is based on experiments, performed on selected ternary metal alloys and silicates, which indicate a linear relationship between practical ion yields and matrix composition.[31-33] Using oxygen flooding in conjunction with a low current density Ar^+ primary beam, the sample surfaces were saturated with oxygen. Thus, the effects of reactive species enhancement were standardized. The remaining matrix-induced variations of practical ion yields were then explained using the expression

$$\tau_M = \Sigma_{i=1}^{n} P_{M,i} C_i \quad (8)$$

where τ_M is the practical ion yield of element M; $P_{M,i}$ is a parameter representing the influence of element i on the ion yield of element M; and C_i is the atomic fraction of element i.

For quantitative analysis based on this approach, relative sensitivity factors were obtained using Eq. (8) to described the practical ion yields of both the analyte and the reference. Relative sensitivity factors obtained by such a calculation were shown to agree with the experimentally determined values to an accuracy of 1 to 7% RSD.[33] Despite the success of this method in the cases studied, it has not been successfully applied to other types of samples. Although the reason for the limited use of the method has not been stated in the literature, it is probably related to the difficulty of saturating nonmetallic surfaces with oxygen.

C. OXIDE BOND APPROACH

The oxide bond explanation of matrix effects is based on the work of Yu and Reuter.[34-35] They performed SIMS analyses on various binary metal alloys under both O_2^+ bombardment and Ar^+ bombardment with oxygen flooding. After the SIMS analyses, the alloys were then analyzed with X-ray photoelectron spectroscopy (XPS) to determine the types of metal oxides formed and the extent of oxidation.

The XPS data from the pure elemental metals revealed that oxidation was more extensive for those metals that form metal oxides with large negative free energies of formation than those metals that form oxides with less favorable free energies of formation. The addition of the second alloy component resulted in significant changes in oxidation, ionization probability, and ion energy distribution for both components. The observed trends can be summarized by two general rules. First, for an alloy A-B, where A forms a stronger oxide bond than B, the presence of A enhances the oxidation and also the ion yield of B, whereas the presence of B suppresses the oxidation and also the ion yield of A. Second, the presence of A sharpens the energy

distribution of B^+, whereas the presence of B broadens the energy distribution of A^+. Both the trends in ion yield and ion energy distribution were attributed to the relative extent of surface oxidation. The influence of surface oxidation has been attributed both to changes in the work function of the surface and also to changes in the bond breaking mechanism of the surface.[36] While these rules were firmly supported by data, they were never applied to any type of matrix effect calibration for quantitative SIMS analysis.

IV. MATRIX EFFECT CALIBRATION FOR $Al_xGa_{1-x}As$ MATRICES

There have been only a few investigations of the influence of matrix effects on the ion yields and sputtering yields of IIIA-VA semiconductors. For homologous series of compounds, such as $Al_xGa_{1-x}As$ and $GaAs_xP_{1-x}$ matrices, under both O_2^+ and Cs^+ bombardment, Katz[37] observed that sputtering yields were linearly related to the changing matrix composition. Similarly, for $Al_xGa_{1-x}As$ matrices under O_2^+ bombardment, others[30,38] have observed that the useful ion yields of major and trace elements were linearly related to the matrix composition defined by x. Although these investigations indicated that linear relationships existed, precise and reproducible matrix effect calibration lines could not be obtained because of the indeterminate variation of instrumental parameters that alter the observed ion yields and sputtering yields between analyses. A method of normalizing these instrumental parameters was required.

The significance of instrumental variations and procedures for normalizing their influence were examined by Galuska and Morrison.[38] Using an O_2^+ primary ion beam, they performed a series of analyses on groups of ion implanted $Al_xGa_{1-x}As$ matrices. To ensure nearly identical analysis conditions during each analysis period, groups of samples, including in each case GaAs, were inserted simultaneously. These samples were sequentially analyzed without manipulating any instrumental parameters. While minimizing instrumental variations in this way, the useful ion yields (τ) of the trace and major elements were obtained. These useful ion yields were then ratioed to produce relative sensitivity factors (RSFs) and relative ion yields ($R\tau$s).

$$R\tau = \tau_x/\tau_o \tag{9}$$

where τ_x is the useful ion yield of the analyte in a particular $Al_xGa_{1-x}As$ matrix, and τ_o is the useful ion yield of the analyte in GaAs when both measurements are performed under nearly identical conditions.

The linearity, precision, and reproducibility of matrix effect calibration lines formed using τ's, RSFs and Rτs were then compared. The results for Be, Si, P, B, and As are presented in Tables 1, 2, and 3. The calibration lines obtained using relative ion yields were the most linear, precise, and reproducible. As expected, the calibration lines obtained using useful ion yields were linear but exhibited poor precision and reproducibility. Despite good reproducibility (~ 24.4%) for a given data point, the relative sensitivity factors resulted in calibration lines with poor linearity, precision, and reproducibility. The superiority of Rτs over RSFs for matrix effect calibration is readily justified. An Rτ is directly proportional to the ion yield of the analyte, whereas an RSF is related to the ion yields of both the analyte and the reference. Because the influence of instrumental variations on the ion yields of the analyte and reference can vary independently, RSFs are altered by instrumental changes to a greater extent than Rτs. Moreover, Rτs are designed to normalize matrix effects to a standard matrix, whereas RSFs are not so designed.

In addition to τ's, RSFs, and Rτs, absolute sputtering yields[5] and relative sputtering yields (RSs) were also determined as a function of matrix composition. As shown in Table 4, the calibration lines obtained using relative sputtering yields (where $RS = S_x/S_o$) were quite precise and reproducible, unlike the absolute sputtering yields. The use of Rτs and RSs has permitted the influence of matrix changes on ion yields and sputtering yields to be precisely calibrated (~ 10% RSD) for the first time.

Table 1. Practical Ion Yield Calibrations for $Al_xGa_{1-x}As$ Matrices[38]

Analyte	Week No.	X Values	Intercept ($\times 10^{-7}$)	Slope ($\times 10^{-5}$)	Linear Correlation (r^2)	RSD Slope (%)
^{9}Be	1	0,0.12,0.26,0.37	1.23	41.5	0.927	32.8
	2	0,0.13,0.21,0.37	116	67.3	0.915	68.6
	3	0,0.13,0.18,0.21	61.4	32.3	0.995	9.5
^{28}Si	1		36.4	22.2	0.989	18.5
	2		25.3	15.2	0.987	17.0
	3		38.9	17.7	0.984	10.8
^{31}P	16	0,0.18,0.26,0.31	0.822	0.291	0.936	18.6
	32	0,0.13,0.18,0.37	1.17	0.258	1.000	2.0
^{11}B	16		25.8	7.05	0.734	53.6
	32		28.2	17.0	0.994	8.7
^{75}As	1		1.78	0.130	0.966	14.6
	2		0.932	0.0891	0.915	21.0
	3		0.940	0.108	0.984	11.0
	32		0.918	0.0532	0.932	11.2
		Av RSD per Point = 18.4%				
^{9}Be	total		31.4	44.7	0.868	12.3
^{28}Si	total		11.0	19.0	0.994	5.8
^{31}P	total	1.00	1.00	0.278	0.928	12.4
^{11}B	total		27.0	15.3	0.825	18.8
^{75}As	total		0.642	0.111	0.722	19.2
		Av RSD per Point = 60.4%				

Table 2. Relative Sensitivity Factor Calibrations for $Al_xGa_{1-x}As$ Matrices[38]

Analyte	Week No.	X Values	Intercept ($\times 10^{-7}$)	Slope ($\times 10^{-5}$)	Linear Correlation (r^2)	RSD Slope (%)
$^{9}Be/^{75}As$	1	0,0.12,0.26,0.37	47.0	890	0.731	33.6
	2	0,0.13,0.21,0.37	84.8	573	0.894	23.0
	3	0,0.13,0.18,0.21	66.5	950	0.995	4.7
$^{28}Si/^{75}As$	1		39.8	271	0.708	38.2
	2		39.4	382	0.903	24.2
	3		36.0	711	0.936	37.8
$^{31}P/^{75}As$	16	0,0.18,0.26,0.31	1.58	9.67	0.715	40.3
	32	0,0.13,0.18,0.37	1.88	4.91	0.827	58.9
$^{11}B/^{75}As$	16		30.7	454	0.945	26.1
	32		60.9	509	0.940	17.1
		Av RSD per Point = 10.4%				
$^{9}Be/^{75}As$	total		88.7	740	0.694	16.8
$^{28}Si/^{75}As$	total		42.7	357	0.804	17.7
$^{31}P/^{75}As$	total		2.41	4.45	0.464	79.2
$^{11}B/^{75}As$	total		34.0	481	0.883	19.2
		Av RSD per Point = 24.4%				

Table 3. Relative Ion Yield Calibrations for $Al_xGa_{1-x}As$ Matrices[38]

Analyte	Week No.	X Values	Intercept ($\times 10^{-7}$)	Slope ($\times 10^{-5}$)	Linear Correlation (r^2)	RSD Slope (%)
^{9}Be	1	0,0.12,0.26,0.37	1.0	52.9	0.999	6.4
	2	0,0.13,0.21,0.37	1.0	42.6	0.996	4.3
	3	0,0.13,0.18,0.21	1.0	41.7	1.000	14.2
^{28}Si	1		1.0	44.5	1.000	9.8
	2		1.0	40.1	0.975	5.7
	3		1.0	45.9	1.000	9.6
^{31}P	16	0,0.18,0.26,0.31	1.0	21.2	0.995	9.6
	32	0,0.13,0.18,0.37	1.0	23.0	1.000	2.5
^{11}B	16		1.0	46.7	0.990	10.7
	32		1.0	39.5	1.000	8.6
^{75}As	1		1.0	6.00	0.933	15.7
	2		1.0	6.54	0.991	2.8
	3		1.0	5.76	0.980	12.4
	32		1.0	5.32	0.925	11.0
		Av RSD per Point = 7.4%				
^{9}Be	total		1.0	46.3	0.981	13.7
^{28}Si	total		1.0	44.7	0.986	5.0
^{31}P	total		1.0	22.1	0.942	4.6
^{11}B	total		1.0	46.6	0.961	7.0
^{75}As	total		1.0	5.76	0.917	7.0
		Av RSD per Point = 9.2%				

Table 4. Relative Sputtering Yield Calibrations For $Al_xGa_{1-x}As$ Matrices[38]

Week No.	Intercept	Slope	Linear Correlation (r^2)	RSD Slope (%)
1	1.0	-1.00	0.928	11.8
2	1.0	-1.01	0.913	12.5
3	1.0	-0.89	0.991	4.0
16	1.0	-0.89	0.997	3.2
32	1.0	-0.75	0.934	11.6
		Av RSD per Point = 3.8%		
total	1.0	-0.86	0.906	8.3
		Av RSD per Point = 7.9%		

V. QUANTITATIVE ANALYSIS OF $Al_xGa_{1-x}As$ MULTILAYERS

Through the use of $R\tau$ and RS calibration lines, the quantitative SIMS analysis of $Al_xGa_{1-x}As$ multilayers (superlattices) has become possible. The only requirement is that a GaAs standard be analyzed under the same conditions as the sample of interest. The concentration of analyte at each point of a depth profile C_p (atom/cm^3) can be determined using Eq. (10).

$$C_p = I_p / R\tau_x \, \tau_o \, z_p \, A_o \tag{10}$$

where $R\tau_x$ is the relative ion yield determined from a calibration line for the appropriate value of x, τ_o is the useful ion yield of the analyte in the standard matrix (GaAs), I_p is the signal, and z_p is the depth increment associated with each point of the depth profile. Similarly, the erosion rate at each point of a depth profile $\overset{o}{z}_p$ can be determined using Eq. (11).

$$\overset{o}{z}_p = RS_x \, \overset{o}{z}_o \, N_o / N_x \tag{11}$$

where RS_x is the relative sputtering yield determined from a calibration line for the appropriate value of x; $\overset{o}{z}_o$ is the sputtering rate of the standard matrix (GaAs); and N_o and N_x are the atomic densities of the standard matrix and the sample, respectively.

The application of Eqs. (10) and (11) requires a knowledge of the matrix composition (x) at each data point. This information is not readily available from an uncalibrated SIMS depth profile. However, a program, superlattice and interface calibration (SLIC),[39] has been developed that determines x at each data point using the $^{75}As^+$ calibration line, the RS calibration line, and the fact that the As concentration is constant in $Al_xGa_{1-x}As$ matrices. If the value of $R\tau_x$ in Eq. (10) is expressed in terms of the equation for the $^{75}As^+$ calibration line ($R\tau_{As,x} = x \, M_{As,R\tau} + 1$, where $M_{As,R\tau}$ is the slope of the line), the equation can be manipulated to the following form:

$$x = \{I_{As,p}/C_{As,p} \cdot A_o \cdot \tau_{As,o} \cdot z_p) - 1\}/M_{As,R\tau} \qquad (12)$$

Except for z_p, the values for all the variables on the right side of Eq. (12) can be readily determined. Because z_p is directly related to $\overset{o}{z}_p$ ($z_p = \overset{o}{z}_p \cdot T_p$, where T_p is the number of seconds per point), it can be expressed in terms of Eq. (11). If RS_x is replaced with the corresponding equation for the RS calibration line, Eq. (13) is obtained

$$\begin{aligned} z_p &= (M_{RS} \cdot x + 1) \cdot \overset{o}{z}_o \cdot N_o/N_x \cdot T_p \\ &= (M_{R\overset{o}{z}} \cdot x + 1) \cdot \overset{o}{z}_o \cdot T_p \end{aligned} \qquad (13)$$

where M_{RS} is the slope of the RS calibration line, and $M_{R\overset{o}{z}}$ is the slope of the corresponding relative erosion rate calibration line ($M_{R\overset{o}{z}} = M_{RS} \cdot N_x/N_0$). Once again the values of z_p and x are the only unknown quantities.

SLIC initially uses the assumption that $x = 0$. The corresponding value of z_p is then determined from Eq. (13) and employed in Eq. (12) to obtain a better approximation of x. This process is reiterated until the values of x and z_p converge. In this manner, the matrix composition and depth at each point of a depth profile are determined through matrix gradients, interfaces, and plateaus. The dopant profiles are then corrected for matrix changes at each data point using Eq. (10) and the appropriate dopant calibration lines.

A 250 keV $^{11}B^+$ implant into a layered sample ($GaAs/Al_{.12}Ga_{.88}As/GaAs$) provides a good example for the correction of matrix effects. In Fig. 2a, the uncorrected SIMS depth profile of $^{11}B^+$ and $^{75}As^+$ in this sample is presented. The first interface occurs at 33 time units, whereas the second interface has not been reached in this profile. Because of matrix effects, the vertical and horizontal scales are no longer linearly related to concentration and depth, respectively. The peak in the $^{11}B^+$ profile at 34 time units is a good example of a distortion introduced by the changing matrix effects at the interface. In Fig. 2b, the horizontal scale has been transformed into depth, and the concentration of Al at each point has been calculated from the $^{75}As^+$ profile. The $^{11}B^+$ profile was then quantified. An

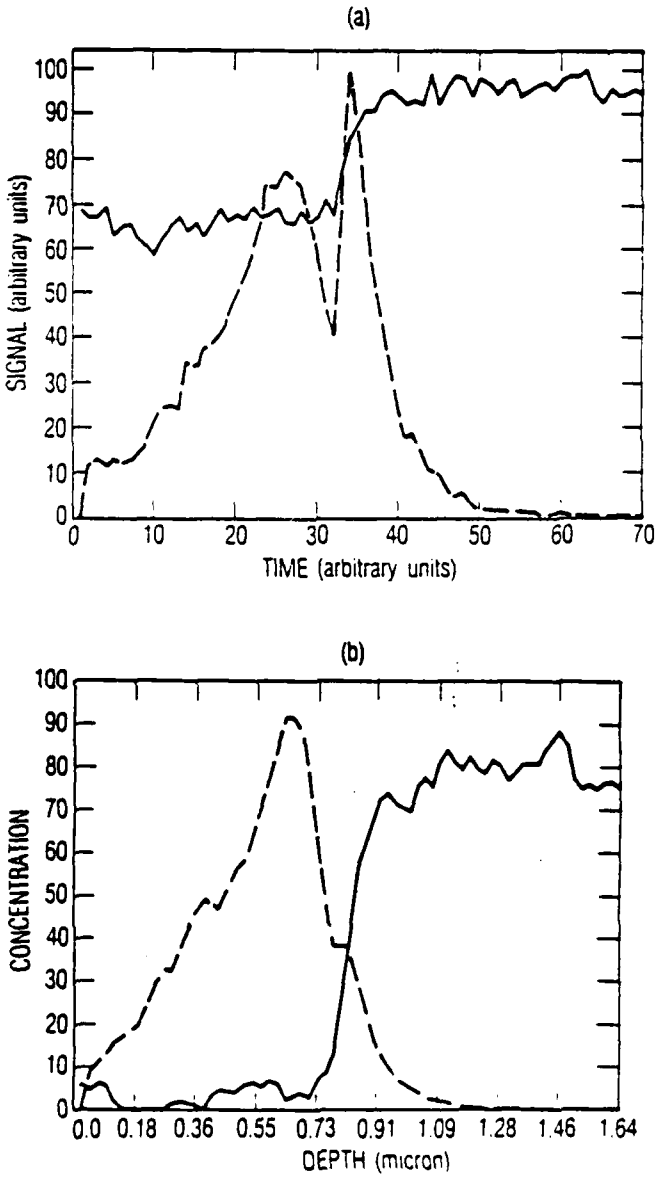

Fig. 2. SIMS Depth Profile of a 250 keV $^{11}B^+$ Implant into a $GaAs/Al_{0.12}Ga_{0.88}As/GaAs$ Sample. (a) Uncorrected profiles of $^{11}B^+$ (---) and $^{75}As^+$ (——); (b) concentration profiles of B(---) (2.0×10^{18} atoms/cm^3 full scale) and Al (——) (1.0×10^{22} atoms/cm^3 full scale).[38]

Al concentration of 2.4×10^{21} atom/cm^3 ± 6.0% was calculated for the $Al_xGa_{1-x}As$ layer, which agrees quite well with the value expected from MBE growth parameters. The correction procedure has also removed the distorted interface region of the $^{11}B^+$ profile, transforming the profile into the slightly distorted Gaussian shape, which was expected.

The most crucial factor influencing the quality of the matrix corrections performed by SLIC is the accuracy with which the matrix structure can be determined. This accuracy has been checked with RBS analysis, which is accurate to about 10% RSD and has a detection limit of 1% for $Al_xGa_{1-x}As$ matrices. In Fig. 3, a complex $Al_xGa_{1-x}As$ sample was analyzed by SIMS and RBS, respectively. The Al concentration at specific regions of the superlattice was determined using SLIC and standard RBS techniques.[40] As shown in Table 5, the values determined by the two techniques agree quite well. In fact, the two sets of data are not statistically different at a 95% confidence level.

In addition to matrix composition, the point-by-point correlation between matrix structure and dopant distribution is critical. Small differences between the actual and the measured matrix structure can significantly influence the corrections performed on dopant distributions. As apparent in Fig. 4, the $^{75}As^+$ signal tracks the Al distribution quite well. This correlation is used by SLIC to precisely determine matrix structures. However, errors can still result from the correlation between matrix structure and dopant distribution. For example, there is a dead time between the measurement of the matrix signal and the dopant signal for each point of a depth profile. When this dead time is large compared to the abruptness of the matrix changes, the matrix and dopant signals will be obtained from different matrix regions. Consequently, the dopant signal will be calibrated for the wrong matrix composition. Such an error is shown in Fig. 5. Fortunately, this type of error can usually be avoided by minimizing the dead time and reducing the sputtering rate.

The full utility of SLIC can be appreciated when very complex samples are analyzed. An uncorrected SIMS depth profile of a complex $Al_xGa_{1-x}As$ super-

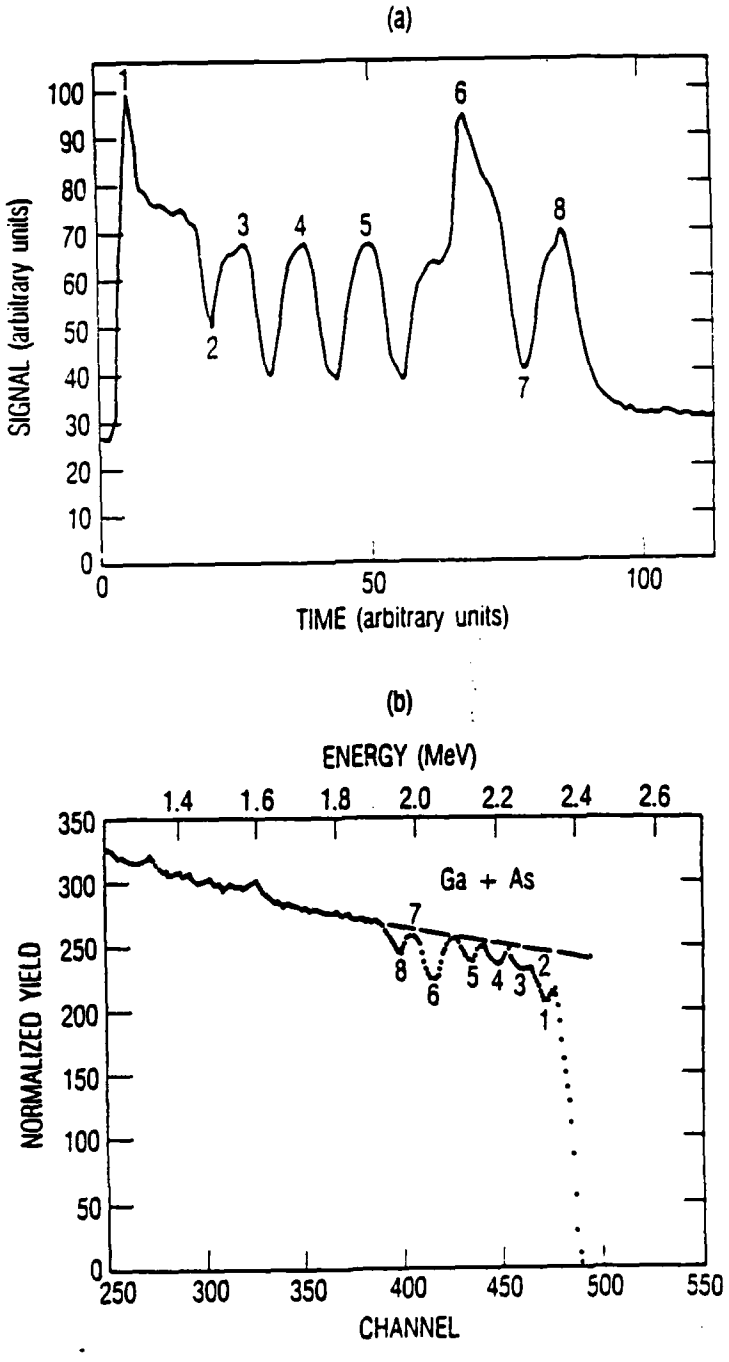

Fig. 3. SIMS and RBS Depth Profiles of an $Al_xGa_{1-x}As$ Superlattice. (a) An Uncorrected $^{75}As^+$ SIMS profile; (b) an RBS profile of the total counts from Ga and As.[39]

Table 5. Point-by-Point Comparison of Al Concentrations Determined by SIMS and RBS Analyses[39]

Point	Al Concentration (X 10^{21} atom/cm^3) RBS	SIMS	Deviation
1	12.0	13.0	-1.0
2	4.2	3.9	+0.3
3	5.1	4.8	+0.3
4	5.1	4.7	+0.4
5	5.2	4.7	+0.5
6	11.0	11.0	0.0
7	1.0	1.3	-0.3
8	4.9	5.7	-0.8
	AVG Deviation = -0.075		

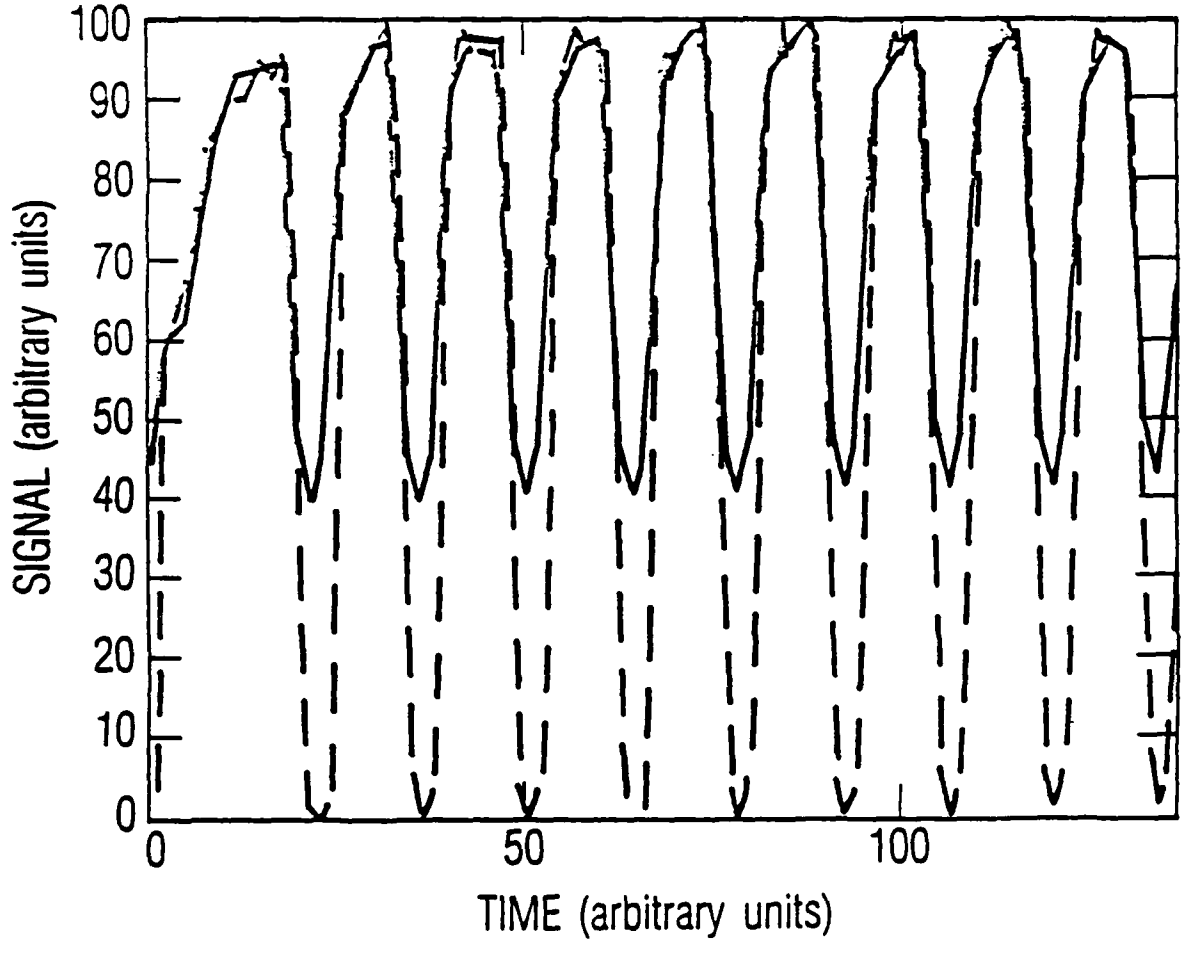

Fig. 4. An Uncorrected SIMS Depth Profile of $^{75}As^{+}$ (——) and $^{27}Al^{2+}$ (---) in an $Al_xGa_{1-x}As$ Superlattice[39]

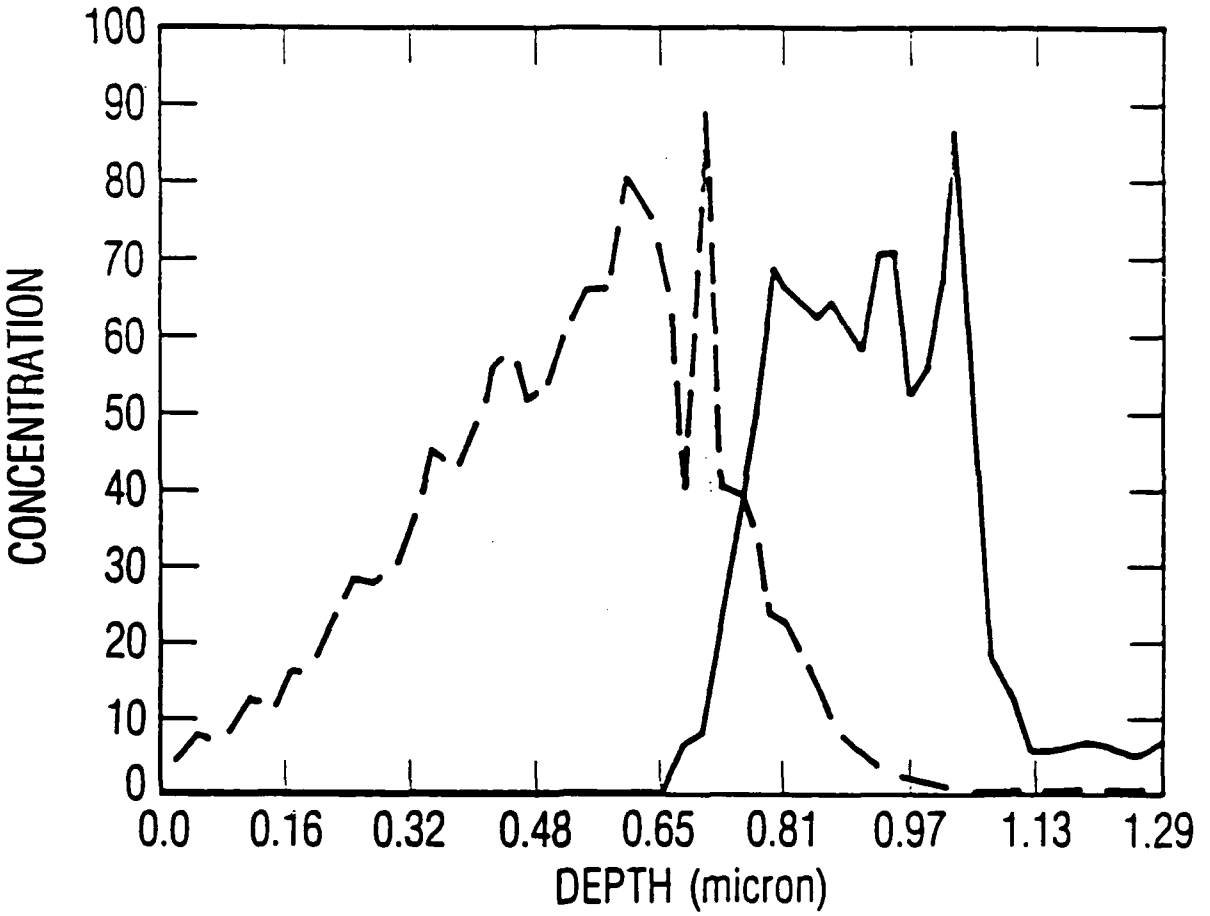

Fig. 5. A Matrix Corrected SIMS Depth Profile of a 250 keV $^{11}B^{+}$ Implant into a GaAs/$Al_{0.30}Ga_{0.70}As$ Sample with a Matrix-Dopant Mismatch at the Interface Located at a Depth of Approximately 0.69 um [B conc. (...) (2×10^{18} atoms/cm^3 full scale) and Al conc. (——) (1×10^{22} atoms/cm^3 full scale)][39]

lattice grown by MBE with Be and Si dopants is presented in Fig. 6a. In Fig. 6b, SLIC has been used to quantify the elemental distributions in this sample. In the uncorrected profile, both the Be and Si distributions follow the $^{75}As^{+}$ signal because of the changing matrix effects. Upon calibration, both the Be and Si distributions have changed substantially. As expected from the MBE growth conditions, the Be concentration generally increases as the Al concentration decreases and vice versa. In addition, excluding the surface buildup, the Si distribution has generally leveled out at 4×10^{18} atom/cm^3. Without SLIC, this type of analysis could not have been made. At the present, SLIC represents the only successful attempt at using SIMS to quantify elemental distributions through multilayers of changing matrix.

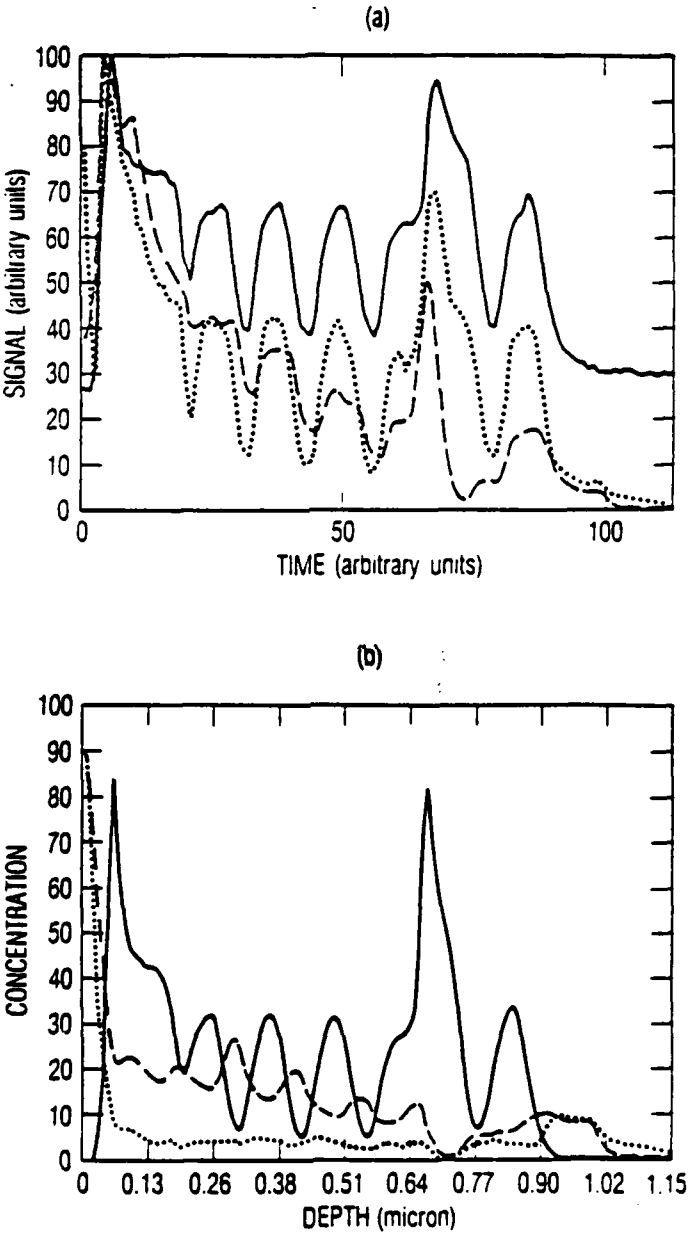

Fig. 6. SIMS Depth Profile of a $Al_xGa_{1-x}As$ Superlattice Doped with Be and Si. (a) Uncorrected profiles of $^{9}Be^{+}$ (——), $^{28}Si^{+}$ (...), and $^{75}As^{+}$ (——); (b) concentration profiles of Be (---) (5.0×10^{19} atoms/cm^3 full scale), Si (...) (9.0×10^{19} atoms/cm^3 full scale), and Al (——) (1.5×10^{22} atom/cm^3 full scale).[39]

VI. EXTENDED MATRIX EFFECT CALIBRATION

Although the initial attempts at matrix effect calibration and correction have been successful for $Al_xGa_{1-x}As$ matrices, the general application of such calibration procedures to a greater variety of matrices requires a better understanding of the fundamental processes involved. During their attempts to extend the $Al_xGa_{1-x}As$ matrix effect calibration lines to other IIIA-VA semiconductors ($Ga_{0.47}In_{.53}As$, GaSb, InSb, InP, GaP, and $Al_xGa_{1-x}As$ matrices were analyzed), Galuska and Morrison[41] examined the applicability of the sputtering yield, compositional, and oxide bond explanations of matrix effects. As in previous analyses, an O_2^+ primary ion beam was used. To reduce experimental errors, practical ion yields and sputtering yields were replaced with R_T and RS, respectively.

The sputtering yield hypothesis was evaluated directly using Eq. (7). The compositional approach was examined in conjunction with the oxide bond approach. The parameter $P_{M,i}$ from Eq. (8) was treated as a measure of the affinity of element i for oxygen. The values of $P_{M,i}$ were approximated from the average bond energies of the diatomic metal oxides.

According to the compositional theory, plots of R_T versus the average matrix-oxygen bond energy should yield straight lines. Similarly, according to the sputtering yield hypothesis, plots of log (R_T) versus log (1/RS) should also yield straight lines. The experimental data for $^{28}Si^+$, plotted using the two different approaches, are presented in Figs. 7a and 7b. As apparent in these figures, the compositional theory satisfies the linearity criteria much better than does the sputtering yield approach. This fact is emphasized in Table 6 where the linear correlations and standard deviations of the lines for several different elements are compared. In each case, excellent linearity and precision were observed when using the compositional approach, and poor linearity and precision were observed when using the sputtering yield approach. This linearity persisted whether the analyses were performed under O_2^+ bombardment or Ar^+ bombardment with oxygen flooding. These experiments demonstrate that the affinity of a matrix for oxygen seems to be

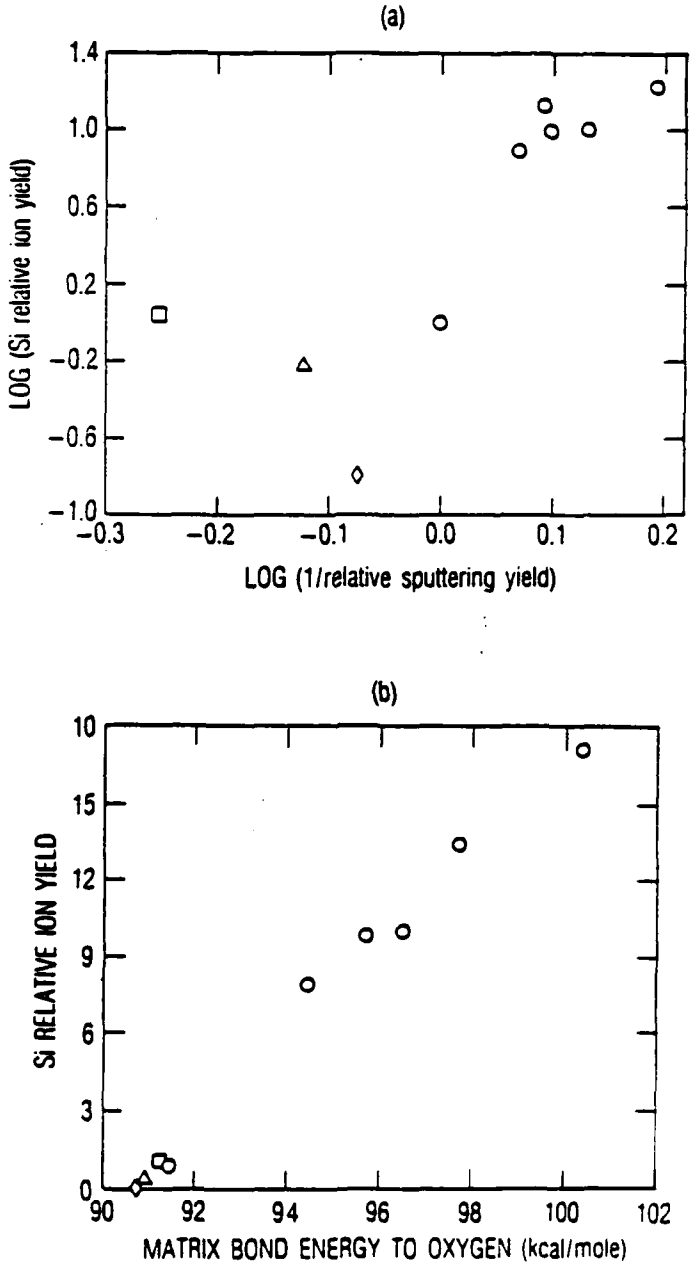

Fig. 7. Influence of Matrix Effects on the τ Value of ^{28}Si. (a) Sputtering yield approach; (b) compositional approach ($Al_xGa_{1-x}As$-O, InP- Δ , InSb- ◊ , GaP- □).[41]

Table 6. Linearity of the Sputtering Yield and Compositional Approaches to Matrix Calibration for Group IIIA-VA Compound Matrices Under O_2^+ Bombardment[41]

Analyte	Linear Correlation (r^2)	RSD Slope (%)
Log (R_T) Versus Log (1/RS)		
$^{28}Si^+$	0.633	64.9
$^{9}Be^+$	0.713	54.1
$^{31}P^+$	0.731	30.8
$^{24}Mg^+$	0.748	21.1
$^{11}B^+$	0.534	32.9
$^{121}Sb^+$	0.791	16.5
R_T Versus Matrix-Oxygen Bond Energy		
$^{28}Si^+$	0.999	0.28
$^{9}Be^+$	0.998	0.42
$^{31}P^+$	0.991	0.24
^{24}Mg	0.993	0.60
$^{11}B^+$	0.998	0.24
$^{121}Sb^+$	0.995	0.29

the critical factor (at least for IIIA-VA semiconductors under O_2^+ bombardment) determining the variation of ion yields with matrix. This oxygen affinity is determined by the matrix composition. Although the sputtering yield does influence the amount of oxygen available for bonding, it does not determine the final oxygen content of the surface.[30]

To determine a general mechanism for matrix effects, it is important to understand how matrix effects influence the τ's of one particular element versus another. One can gain an insight into this phenomenon by comparing the slopes of the calibration lines to the first ionization potentials of the respective analytes. Such a comparison is presented in Table 7. For those elements that fall in the same column of the periodic table [(B, Al, Ga), (P, As, Sb), and (Be and Mg)], a general relationship is observed. Elements with larger first ionization potentials yield calibration lines of steeper slope than those with smaller first ionization potentials. This indicates that elements that have larger ionization potentials (small ionization probability) are influenced by matrix effects (the amount of bound oxygen) to a greater extent than those that have smaller ionization potentials (large ionization probability). As one might expect, this relationship is very similar to that commonly observed for elemental τ's in a single matrix enhanced by oxygen bombardment or flooding: the τ's of elements with small ionization probabilities are enhanced to a greater extent by the presence of oxygen than those of elements with large ionization probabilities.

The excellent linearity of the $R\tau$ versus matrix-oxygen bond energy calibration lines and the relationship of the lines to elemental ionization potentials can be used to improve the quality of both qualitative and quantitative SIMS analysis. Using the relationships expressed in these matrix calibration lines, one can anticipate when matrix effects will be a problem, and how they may distort depth profiles of layered multimatrix samples. For example, a largely distorted Gaussian depth distribution would be expected for the SIMS analysis of an $^{11}B^+$ implant through a GaAs layer into an $Al_{.30}Ga_{.70}As$ layer because $^{11}B^+$ emission is very sensitive to the presence of oxygen, i.e., matrix effects, and $Al_{.30}Ga_{.70}As$ has a much greater oxygen affinity than GaAs. Alternatively, a smaller distortion would be expected for a $^{24}Mg^+$

Table 7. Dependence of Rτ Versus Bond Energy Line Slopes on First Ionization Potential[41]

Analyte	Slope	Intercept	1st Ionization Potential (eV)
$^{11}B^+$	1.90	-173	8.30
$^{27}Al^+$	0.19	-17	5.98
$^{69}Ga^+$	0.25	-22	6.00
$^{31}P^+$	0.93	-84	11.02
$^{75}As^+$	0.30	-26	9.81
$^{121}Sb^+$	0.30	-26	8.64
$^{9}Be^+$,	1.86	-169	9.32
$^{24}Mg^+$	0.52	-47	7.64
$^{28}Si^+$	1.88	-170	8.15
$^{7}Li^+$	0.10	-9	5.39

implant and an even smaller distortion for a $^{7}Li^{+}$ implant into such a structure. The sensitivity of the τ's of these elements to matrix effects decreases going from $^{11}B^{+}$ to $^{24}Mg^{+}$ to $^{7}Li^{+}$. The SIMS analyses of these implants are shown in Fig. 8.

These calibration lines are even more valuable when a quantitative SIMS analysis in either a single matrix or a layered multimatrix sample is desired. Because these types of calibration lines are highly reproducible, dopant distributions in a homogeneous group IIIA-VA compound matrix can be quantified using the calibration lines and a single standard prepared from any of the group IIIA-VA compound matrices. There is no need to make a separate standard for each matrix. As shown previously for $Al_xGa_{1-x}As$ matrices, these calibration lines also make possible the quantitative SIMS analysis of layered multimatrix samples. When the criteria necessary for SLIC are satisfied (for a homologous series of compounds such as $Al_xGa_{1-x}As$, $GaAs_xP_{1-x}$, and $InAs_xSb_{1-x}$), very complex layered multimatrix samples may be quantitatively analyzed. When SLIC is not applicable, simpler structures with just a few well defined interfaces may be quantitatively analyzed by treating the interfaces as linear concentration gradients from one matrix (of predetermined composition) to another (the matrix-by-matrix approach). Both approaches have been applied to the hypothetical MBE structure illustrated in Fig. 9a. A $^{9}Be^{+}$ concentration plateau approximately 0.1 μm wide and 1-2 x 10^{18} atom/cm^3 high was grown by MBE while the matrix was linearly changed from GaAs to $Al_{.30}Ga_{.70}As$. In the uncorrected profile, Fig. 9b, the ^{9}Be distribution (dashed line) resembles a sharp spike rather than a plateau. In addition, the thickness and maximum concentration of the plateau cannot be determined. The matrix corrected depth profiles using the matrix-by-matrix approach and SLIC are presented in Figs. 9c and 9d, respectively. The shape of the plateau differs slightly between the two versions of the corrected profile. However, both types of corrections permit a dramatic improvement over the uncorrected profile in the determination of plateau thickness and maximum concentration.

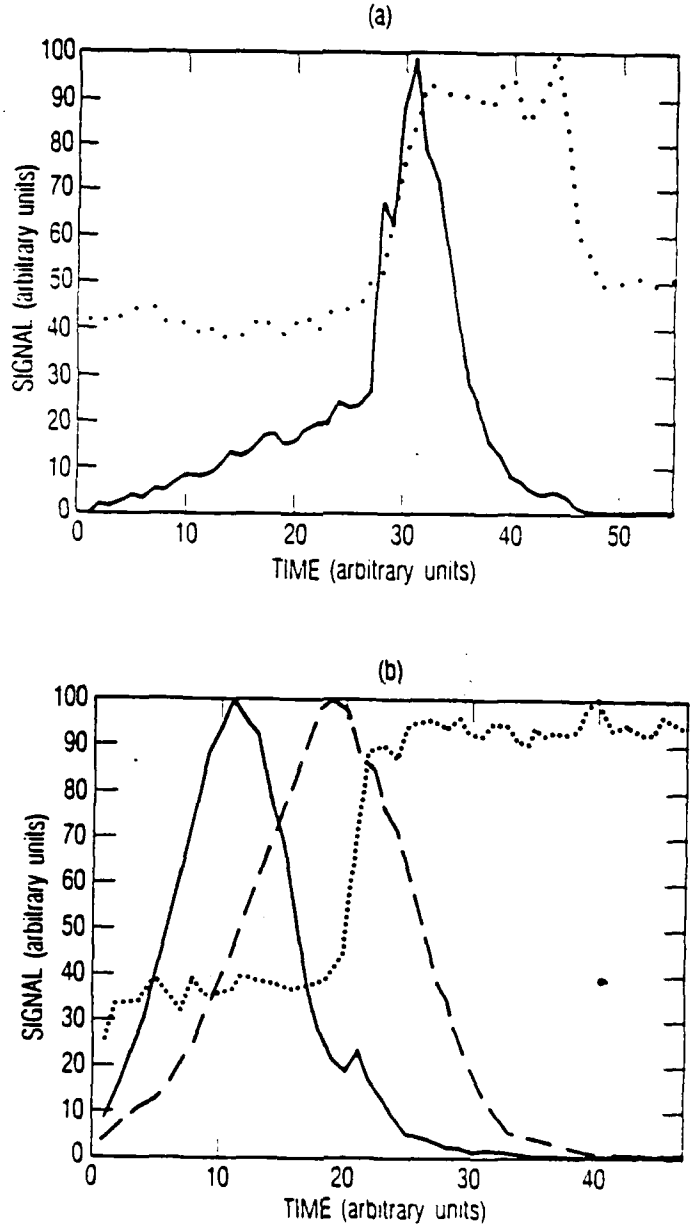

Fig. 8. SIMS Analysis of $^{11}B^+$, $^{24}Mg^+$, and $^{7}Li^+$ Implants Through a GaAs/$Al_{0.3}Ga_{0.7}As$ Structure. (a) Depth profiles of $^{11}B^+$ (...) and $^{75}As^+$ (——) (interface at 31 time units); (b) depth profiles of $^{24}Mg^+$ (——), $^{7}Li^+$ (---) and $^{75}As^+$ (...) (interface at 20 time units).[41]

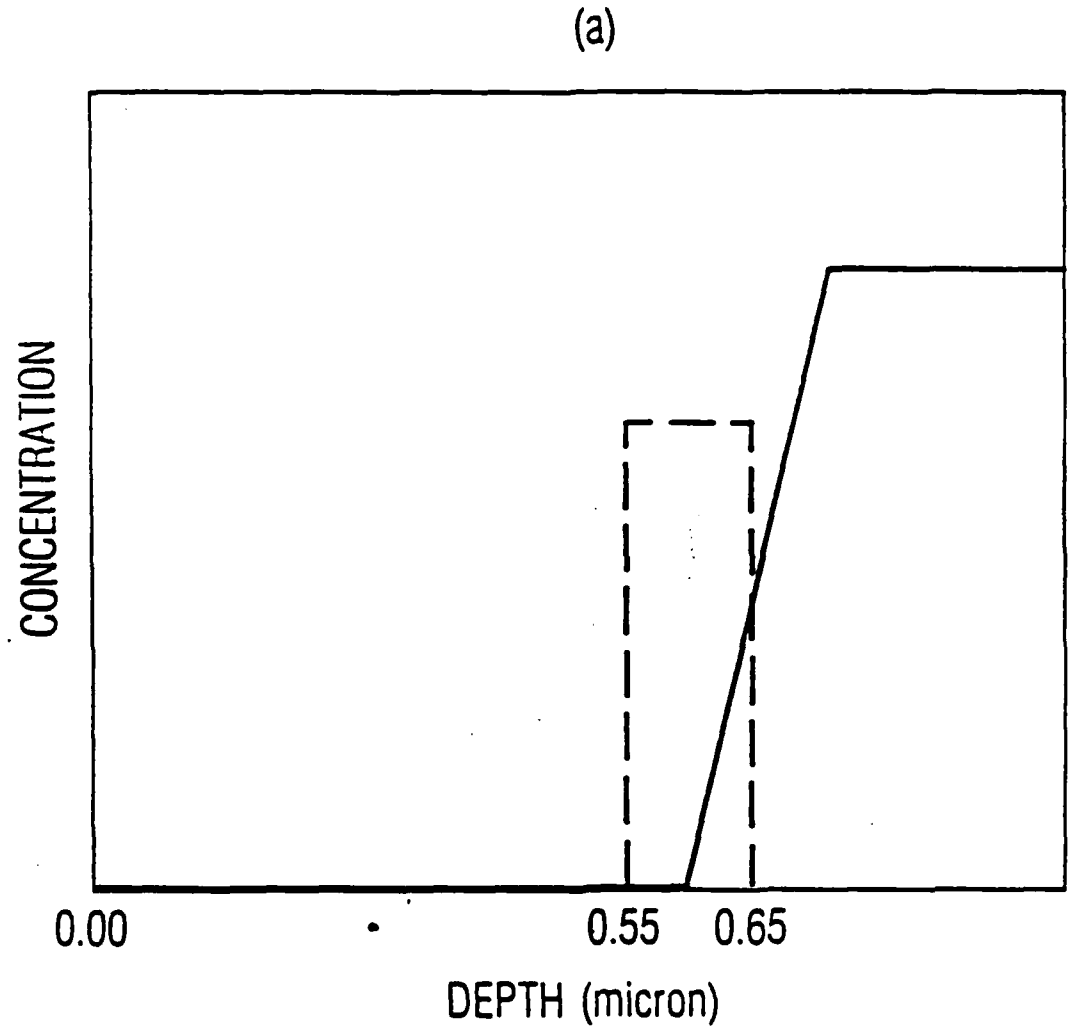

Fig. 9. SIMS Analysis of a Be Plateau at a Graded GaAs/$Al_{0.3}Ga_{0.7}As$ Interface. (a) Hypothetical structure Be (——) (1.2×10^{18} atom/cm^3 peak conc.) and Al (——) (6.7×10^{21} atom/cm^3 peak conc.).

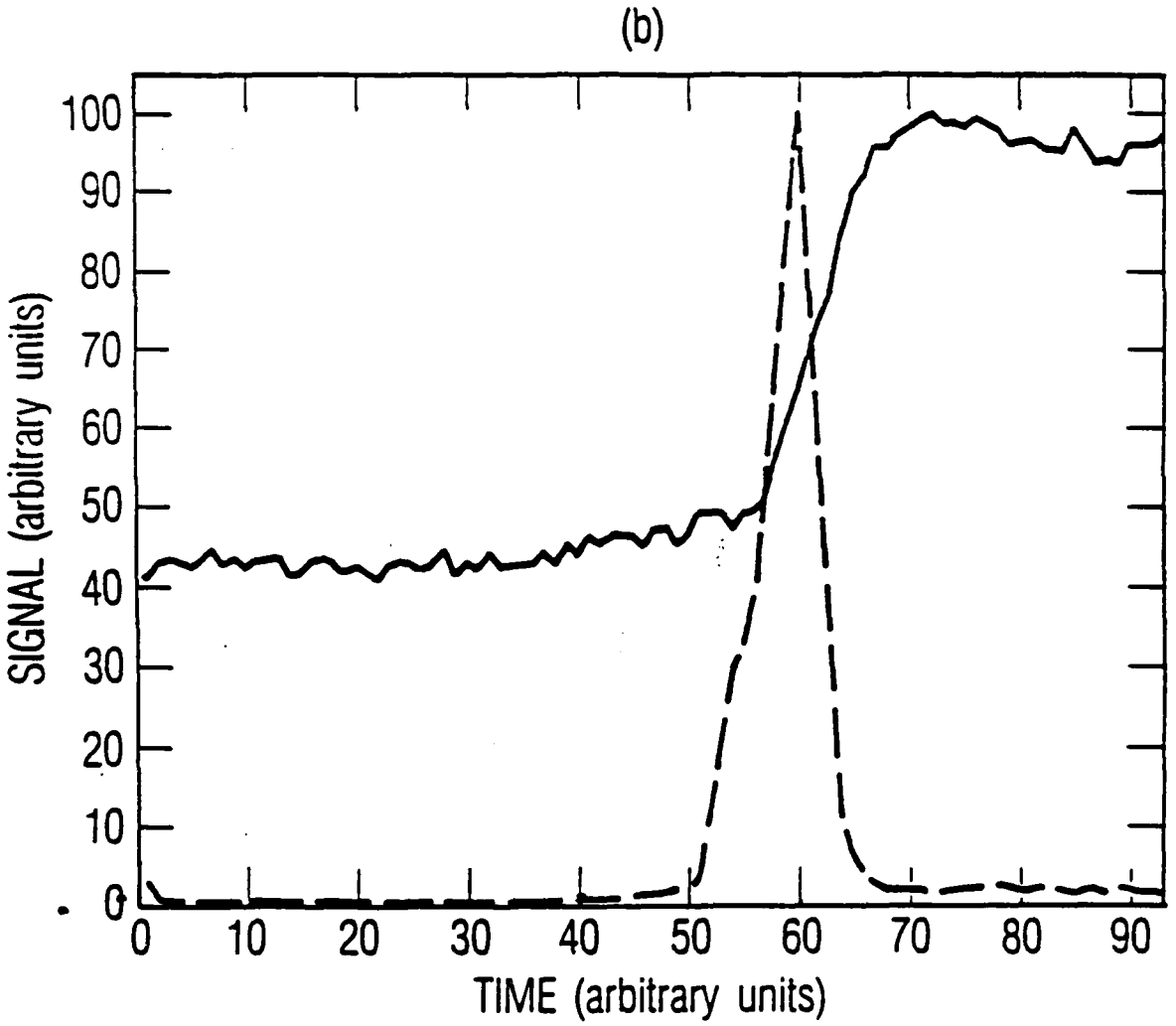

Fig. 9. SIMS Analysis of a Be Plateau at a Graded GaAs/$Al_{0.3}Ga_{0.7}As$ Interface. (b) Uncorrected profile of Be^+ (——) and $^{75}As^+$ (——).

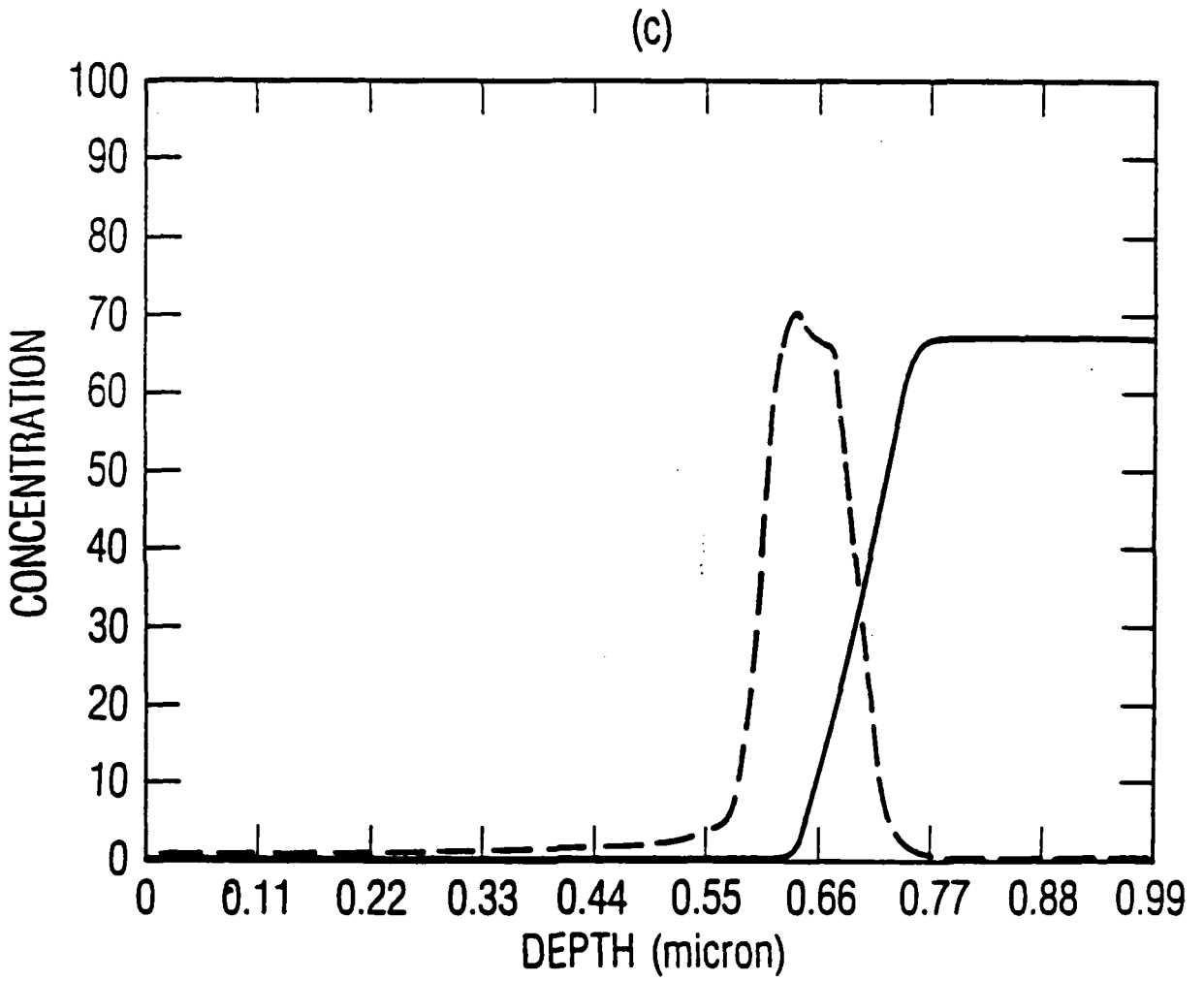

Fig. 9. SIMS Analysis of a Be Plateau at a Graded GaAs/$Al_{0.3}Ga_{0.7}As$ Interface. (c) Corrected profiles of Be (——) (2×10^{18} atom/cm^3 full scale) and Al (——) (1×10^{22} atom/cm^3 full scale) obtained assuming a linear concentration gradient at the interface.

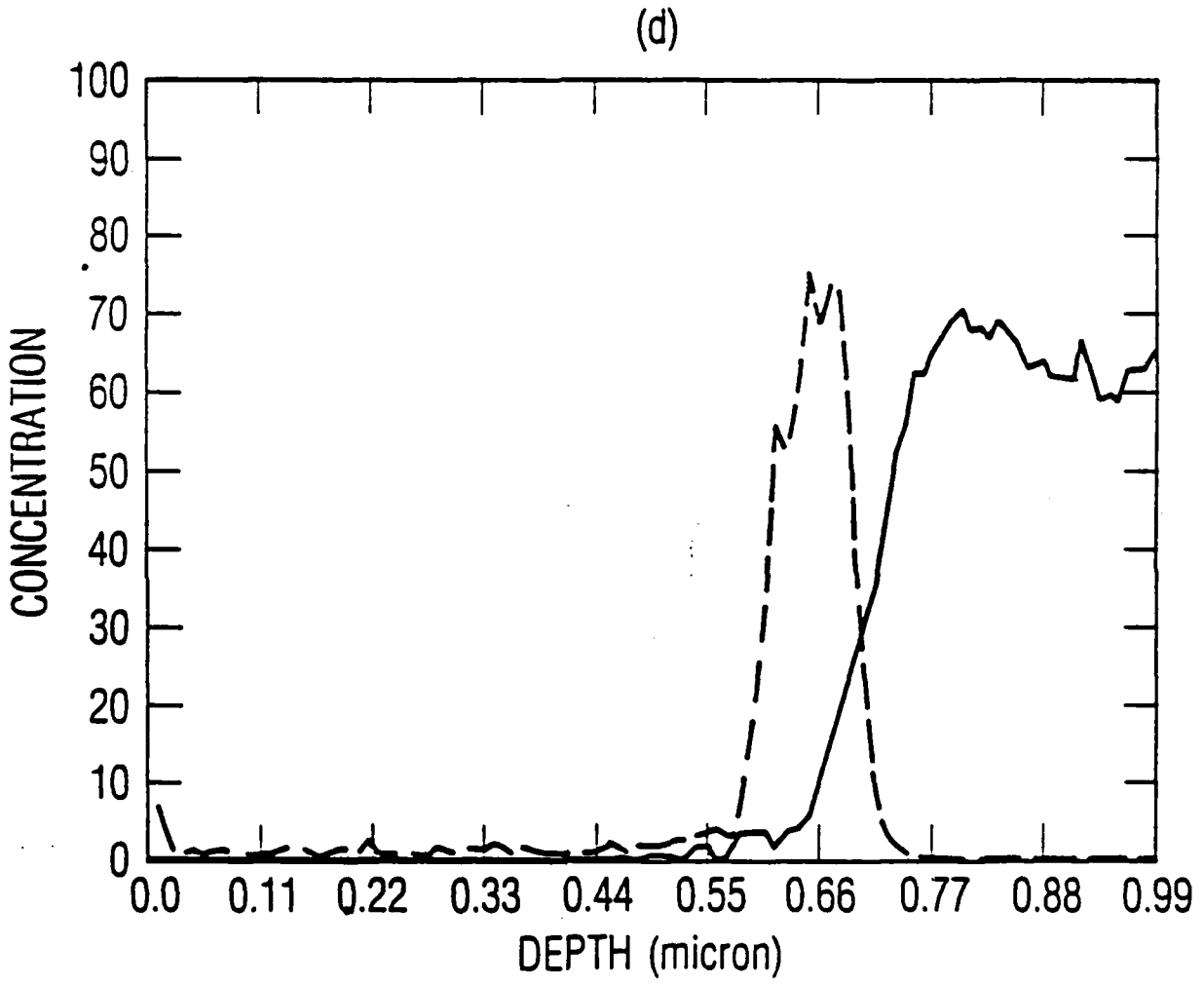

Fig. 9. SIMS Analysis of a Be Plateau at a Graded GaAs/$Al_{0.3}Ga_{0.7}As$ Interface. (d) Corrected profiles of Be (---) (2×10^{18} atom/cm^3 full scale) and Al (——) (1×10^{22} atom/cm^3 full scale) obtained using the program SLIC.

VII. FUTURE TRENDS

These initial investigations into the calibration of the SIMS matrix effects for the quantitative analysis of multilayers of IIIA-VA semiconductors have established the groundwork for future investigations. In particular, five important points have been made. First, both ion yields and sputtering yields were shown to vary linearly with the matrix composition of $Al_xGa_{1-x}As$ and similar series of IIIA-VA semiconductors. Second, matrix calibration lines were shown to have superior precision and reproducibility when relative ion yields and relative sputtering yields were used instead of useful ion yields, relative sensitivity factors, and sputtering yields. Third, a procedure for the quantitative SIMS analysis of multilayer-multimatrix samples has been established and incorporated into the program SLIC. Fourth, the investigation into the factors influencing matrix effects in group IIIA-VA semiconductors revealed that relative ion yield variations with matrix are a linear function of the matrix composition and are influenced primarily by the oxygen affinity of the matrix constituents. Fifth, for elements in the same column of the periodic table, the influence of matrix effects on relative ion yields was shown to increase as the first ionization potential of the analyte increased.

Although these accomplishments represent a significant advance in the development of quantitative SIMS analysis, matrix effect calibration, depth profile correction, and the mechanisms of matrix effects should all be examined in much greater detail. Because of the large inconsistency in the ion and sputtering yields obtained by any given laboratory, these parameters cannot be evaluated critically in the open literature. As a result, progress in the understanding of the sputtering and ion emission processes has been extremely slow. This difficulty could be minimized through the use of the more reproducible relative ion yield and sputtering yield values. Thus, it should be common practice to report R_T and RS values for all materials being examined by SIMS. When so doing, a single material (perhaps silicon) should be established internationally as the standard matrix for normalization.

Thus, ion yields and sputtering yields obtained by different laboratories could be more readily compared and correlated. In particular, the Rτs and RSs of homologous matrices, such as metal silicides and germanides, should be examined for linear relationships like those established for the IIIA-VA semiconductors.

Any procedure for quantifying SIMS depth profiles through multimatrix films must consist of three steps: matrix identification, sputtering rate determination, and ion yield calibration. Although each of these steps can be performed simultaneously by SLIC, the procedure used in SLIC to determine the matrix composition requires the presence of a single element (such as As in $Al_xGa_{1-x}As$) of known concentration in each of the layers. This requirement is not generally satisfied. Thus, a general method of matrix determination through layers is required to complement the matrix effect calibration. One possible solution is the use of a second analytical technique (such as RBS or AES) to determine matrix composition and structure while matrix calibrated SIMS is used to determine the dopant distributions. As previously mentioned, small mismatches in the matrix and trace element depth distributions can result in large errors in the matrix corrected trace element distributions. Thus, the critical factor in such a dual analysis approach is a coherent depth distribution match between the two data sets. Methods of ensuring an adequate registration between the two data sets need to be developed.

The reproducible nature of Rτs should be exploited to determine mechanisms for the influence of matrix effects on practical ion yields. The data indicate that τ's are a function of matrix composition and also the surface concentration of reactive primary species (oxygen and cesium). The surface concentration of reactive species depends on the availability of these species through surface adsorption and implantation during ion bombardment, and also on the oxygen affinity of the matrix. However, little work has been done to determine the relative importance of these factors and how experimental parameters may be altered to permit matrix calibration for a wider variety of samples. The contribution of adsorption, implantation, and matrix composition must be deconvoluted so that matrix effects observed for a variety of samples and analysis conditions may be understood.

REFERENCES

1. H. E. Beske, Z. NaturForch, 22, 459 (1967).

2. Z. Jurela, in Atomic Collision Parameters in Solids, Eds., D. W. Palmer, M. W. Thompson, and P. D. Townsend, North-Holland, Amsterdam (1970), p. 34.

3. G. M. McCracken, Rep. Prog. Phys. 38, 241 (1975).

4. G. Blaise and M. Bernheim, Surf. Sci. 47, 324 (1975).

5. C. A. Andersen, Int. J. Mass Spectrom. Ion Phys. 3, 413 (1970).

6. H. A. Storms, K. F. Brown, and J. D. Stein, Anal. Chem. 49, 2023 (1977).

7. K. Wittmaack, Rad. Eff. 63, 205 (1982).

8. S. Hofman, Appl. Phys. 13, 205 (1977).

9. P. H. Holloway and R. S. Bhattacharya, Surf. Interface Anal. 3, 118 (1981).

10. H. H. Anderson, in Physics of Ionized Gases, Ed., V. Vujnovic, Institute of Physics, Zagreb (1974), p. 361.

11. Z. L. Liau, J. E. Lewis, H. S. Wildman, and J. K. Howard, Surf. Sci. 57, 393 (1976).

12. C. A. Anderson and J. R. Hinthorne, Anal. Chem. 45, 142 (1973).

13. A. E. Morgan and H. W. Werner, Anal. Chem. 48, 699 (1976).

14. Z. Jurela, Int. J. Mass Spectrom. Ion Phys. 37, 67 (1981).

15. Z. Sroubek, Surf. Sci. 44, 47 (1974).

16. J. M. Schroeer, T. N. Rhodin, and R. C. Bradley, Surf. Sci. 34, 571 (1973).

17. W. H. Gries and W. L. Rauternbach, Sixth Int. Symp. Microtechniques, Graz, Austria, 1970.

18. W. H. Gries and E. Norval, Anal. Chim. Acta 75, 289 (1975).

19. D. P. Leta and G. H. Morrison, Anal. Chem. 52, 277 (1980).

20. D. P. Leta and G. H. Morrison, Anal. Chem. 52, 514 (1980).

21. V. R. Deline, C. A. Evans, and P. Williams, Appl. Phys. Lett. 33, 578 (1978).

22. V. R. Deline, C. A. Evans, W. Katz, and P. Williams, Appl. Phys. Lett. 33, 832 (1978).

23. J. E. Chelgren, W. Katz, V. R. Deline, C. A. Evans, R. J. Blattner, and P. Williams, J. Vac. Sci. Technol. 16, 324 (1979).

24. F. Schultz and K. Wittmaack, Rad. Eff. 29, 31 (1976).

25. H. Liebl. J. Vac. Sci. Technol. 12, 385 (1975).

26. P. V. Chu, Doctoral Thesis, Cornell University, 1983.

27. K. Wittmaack, J. Appl. Phys. 52, 527 (1981).

28. K. Wittmaack, Appl. Surf. Sci. 9, 315 (1981).

29. A. E. Morgan, H. A. M. Grefte, and H. J. Tolle, J. Vac. Sci. Technol. 18, 164 (1981).

30. C. Meyer, M. Maier, and D. Bimberg. J. Appl. Phys. 54, 2627 (1983).

31. J. C. Pivin, C. Roques-Carmes, and G. Slodzian, Int. J. Appl. Phys. 51, 4158 (1950).

32. J. C. Pivin, C. Roques-Carmes, and G. Slodzian, J. Appl. Phys. 51, 4158 (1980).

33. A. Havette and G. Slodzian, J. Microsc. Spectrosc. Electron. 5, 131 (1980).

34. M. Yu and W. Reuter, J.Appl. Phys. 52, 1478 (1981).

35. M. Yu, and W. Reuter, J. Appl. Phys. 52, 1489 (1981).

36. K. Wittmaack, Surf. Sci. 112, 168 (1981).

37. W. Katz, Doctoral Thesis, University of Illinois, 1978.

38. A. A. Galuska and G. H. Morrison, Anal. Chem. 55, 2051 (1983).

39. A. A. Galuska and G. H. Morrison, Anal. Chem. 56, 74 (1984).

40. J. W. Mayer, J. F. Ziegler, L. L. Chang, R. Tsu, and L. Esaki, J. Appl. Phys. 44, 2322 (1973).

41. A. A. Galuska and G. H. Morrison, Int. J. Mass Spectrum. Ion Processes 61, 59 (1984).

LABORATORY OPERATIONS

The Aerospace Corporation functions as an "architect-engineer" for national security projects, specializing in advanced military space systems. Providing research support, the corporation's Laboratory Operations conducts experimental and theoretical investigations that focus on the application of scientific and technical advances to such systems. Vital to the success of these investigations is the technical staff's wide-ranging expertise and its ability to stay current with new developments. This expertise is enhanced by a research program aimed at dealing with the many problems associated with rapidly evolving space systems. Contributing their capabilities to the research effort are these individual laboratories:

Aerophysics Laboratory: Launch vehicle and reentry fluid mechanics, heat transfer and flight dynamics; chemical and electric propulsion, propellant chemistry, chemical dynamics, environmental chemistry, trace detection; spacecraft structural mechanics, contamination, thermal and structural control; high temperature thermomechanics, gas kinetics and radiation; cw and pulsed chemical and excimer laser development including chemical kinetics, spectroscopy, optical resonators, beam control, atmospheric propagation, laser effects and countermeasures.

Chemistry and Physics Laboratory: Atmospheric chemical reactions, atmospheric optics, light scattering, state-specific chemical reactions and radiative signatures of missile plumes, sensor out-of-field-of-view rejection, applied laser spectroscopy, laser chemistry, laser optoelectronics, solar cell physics, battery electrochemistry, space vacuum and radiation effects on materials, lubrication and surface phenomena, thermionic emission, photosensitive materials and detectors, atomic frequency standards, and environmental chemistry.

Computer Science Laboratory: Program verification, program translation, performance-sensitive system design, distributed architectures for spaceborne computers, fault-tolerant computer systems, artificial intelligence, microelectronics applications, communication protocols, and computer security.

Electronics Research Laboratory: Microelectronics, solid-state device physics, compound semiconductors, radiation hardening; electro-optics, quantum electronics, solid-state lasers, optical propagation and communications; microwave semiconductor devices, microwave/millimeter wave measurements, diagnostics and radiometry, microwave/millimeter wave thermionic devices; atomic time and frequency standards; antennas, rf systems, electromagnetic propagation phenomena, space communication systems.

Materials Sciences Laboratory: Development of new materials: metals, alloys, ceramics, polymers and their composites, and new forms of carbon; nondestructive evaluation, component failure analysis and reliability; fracture mechanics and stress corrosion; analysis and evaluation of materials at cryogenic and elevated temperatures as well as in space and enemy-induced environments.

Space Sciences Laboratory: Magnetospheric, auroral and cosmic ray physics, wave-particle interactions, magnetospheric plasma waves; atmospheric and ionospheric physics, density and composition of the upper atmosphere, remote sensing using atmospheric radiation; solar physics, infrared astronomy, infrared signature analysis; effects of solar activity, magnetic storms and nuclear explosions on the earth's atmosphere, ionosphere and magnetosphere; effects of electromagnetic and particulate radiations on space systems; space instrumentation.

END

12-86

DTIC